Research

Author for correspondence:
Leonardo L. Gollo
e-mail: leonardo.l.gollo@gmail.com

The frustrated brain: from dynamics on motifs to communities and networks

Leonardo L. Gollo[1] and Michael Breakspear[1,2,3]

[1]Systems Neuroscience Group, QIMR Berghofer Medical Research Institute, Brisbane, Queensland, Australia
[2]School of Psychiatry, University of New South Wales and The Black Dog Institute, Sydney, New South Wales, Australia
[3]The Royal Brisbane and Women's Hospital, Brisbane, Queensland, Australia

Cognitive function depends on an adaptive balance between flexible dynamics and integrative processes in distributed cortical networks. Patterns of zero-lag synchrony likely underpin numerous perceptual and cognitive functions. Synchronization fulfils integration by reducing entropy, while adaptive function mandates that a broad variety of stable states be readily accessible. Here, we elucidate two complementary influences on patterns of zero-lag synchrony that derive from basic properties of brain networks. First, mutually coupled pairs of neuronal subsystems—resonance pairs—promote stable zero-lag synchrony among the small motifs in which they are embedded, and whose effects can propagate along connected chains. Second, frustrated closed-loop motifs disrupt synchronous dynamics, enabling metastable configurations of zero-lag synchrony to coexist. We document these two complementary influences in small motifs and illustrate how these effects underpin stable versus metastable phase-synchronization patterns in prototypical modular networks and in large-scale cortical networks of the macaque (CoCoMac). We find that the variability of synchronization patterns depends on the inter-node time delay, increases with the network size and is maximized for intermediate coupling strengths. We hypothesize that the dialectic influences of resonance versus frustration may form a dynamic substrate for flexible neuronal integration, an essential platform across diverse cognitive processes.

1. Introduction

Understanding large-scale cortical dynamics and their relationship to the underlying anatomy is key to unlocking the computational principles of the brain. Despite cytological differences at the microscopic level, the repetitive design of mesoscopic motifs—circuits, columns and local hierarchies—is a stand-out feature of brain anatomy. By promising a way of scaling up in size, this repetitive principle is likely crucial to the success of the very large-scale computational modelling efforts currently underway. From this view, it is the larger scale structural connectivity and topological constraints of macroscopic anatomy that plays the crucial role in sculpting information processing in the cortex [1,2]. According to this modern connectionist approach, the anatomical network is fundamental because the functionally specialized and integrative roles of cortical regions come from their interactions with other brain regions, not only from their microscopic particularities. Functional network is a widely used approach to study one of the major current paradigms of neuroscience: the relationship between structure and dynamics [3]. While the physical structure remains roughly constant on the time scale of minutes to hours, the dynamic states of cortical regions evolve in a coordinated way to perform a multitude of tasks, which vary on far shorter time scales. Although some states of brain dynamics are very general and common, at least among individuals of a same species, others are very particular, and perhaps unique.

Spanning different neuronal scales, synchronization is an important dynamical feature that can increase the effectiveness of interactions between brain regions, for example by aligning neuronal spikes from different regions into critical windows for spike-time-dependent plasticity [4]. Indeed, an emerging

paradigm considers synchronization as *the* key feature that modulates cortical interactions [5]: accordingly, its maximum effectiveness is achieved when two mutually interacting areas are phase coupled. The synchronization strength between regions is thus fundamental, and a functional network is composed of nodes that are linked by highly correlated pairs. The interactions between brain regions, in turn, are not static but rather erratic, depending on their dynamics and past activity [6–8]. Such a dynamic balance of integration and instability likely underlies the need for cortical function to switch according to the changing environmental needs [9–11]. Hence, variable and flexible dynamics, which depends on coupling delay [12] and the balance of excitation and inhibition [13], is a hallmark of adaptive cognitive behaviour.

Understanding dynamic functional networks is not only an important topic, but also a rather complex one. As with any problem endowed with complexity, a wise strategic approach is required. A standard way to reduce the level of complexity is to divide the problem into pieces. Often, however, it is not clear which is the best way to split the problem. Neuronal systems are clearly more than the sum of their parts: extrapolations thus demand careful analysis. The fingerprints of small motifs have already become a standard procedure to understand the structure of complex networks [14–19]. A recent, promising approach to understanding the relationship between structure/dynamics on complex networks consists of studying the structure/dynamics relationship in network motifs [20–23]. This rests on the premise that the dynamical features of network motifs plays a role in shaping the dynamics and synchronization of complex networks [21,22].

The connections between cortical regions in the brain, as derived from the primate cortical network, obey a few general principles that may inform the study of structure/dynamic analyses [24]: first, the brain topology is hierarchical with cortical regions occupying the highest positions in the hierarchy [25–27]. Second, spatial clustering leads to a modular architecture, in which nodes are strongly interconnected with regions within the same cluster (SC)—typically nearby in space—than with regions outside their cluster [28,29]. Third, some nodes can be classified as hubs because they have a degree larger than the average node degree of the network [17,30–32]. These principles have been linked to evolutionary and functional advantages as well as optimization arising from the physical and metabolic constraints under which brains operate on evolutionary time scales [33,34]. These general network properties can also shape the dynamics and synchronization of cortical networks [35–37]. However, a complete understanding of how the structural constraints of the anatomical connectivity influence dynamics is lacking, particularly regarding the mechanisms underlying the variability of synchronization.

Here, we analyse the synchronization patterns as they arise in small motifs, prototypical modular structures and cortical networks. We aim to identify factors that enrich the landscape of synchronized cortical states. The paper is structured as follows: in §2 we describe mesoscopic dynamics as they arise from small motifs of coupled neural masses. In §3 we retrace recent work that highlights the stablizing role of reciprocally coupled pairs (which we call resonance pairs) on the motifs (small subnetworks of three nodes) in which they are embedded. This influence is contrasted with that of closed loops, which introduce frustration into the system. Frustrated motifs hence disrupt stability and

synchrony, introducing metastability and variability. In §4−6 we study these two competing influences in small constructed modular networks. Subsequently in §7 we examine structural networks derived from tracing studies of the macaque brain, using the distribution of motifs to link the observed dynamics to those on our prototypical networks.

2. Neuronal network dynamics

We employed numerical methods to study neuronal dynamics on large-scale cortical networks. Each node was considered as a conductance-based neural mass model [36,38,39], described in detail in appendix A. This approach reduces the dimensionality of a cortical region in each node to three nonlinear differential equations, which govern the dynamics of the excitatory subpopulation, the inhibitory subpopulation and the fraction of open potassium channels. Analysis of such a reduced model is required to render the problem of large-scale cortical dynamics tractable. Distributed cortical regions are coupled together through long-range excitatory connections with a delay of 10 ms (unless otherwise stated) to account for finite axonal conduction speed [40]. In our mesoscale model, the dynamic variables start from random initial conditions. Exploring the phase space can lead to different basins of attraction and different transient dynamics, causing considerable trial-to-trial variability, consistent with experiments [41–43]. This variability is an intrinsic feature of many large-dimensional systems. Occasionally, such variability can also arise from transitions between metastable states. The following results should not be interpreted as deterministic outcomes of the model, but instead as likely statistical outcomes revealed through a large number of repetitions of the same numerical experiment. Deeper statistical features, in contrast, are remarkably persistent. For instance, nodes oscillate with two dominant frequencies, a slow approximately 10 Hz and a fast approximately 100 Hz time scale, and two mutually coupled nodes typically synchronize in anti-phase synchrony [23].

3. Resonance pairs in frustrated motifs promote variable synchronization patterns

We begin our analysis by focusing on three-node motifs, whose enumeration (M1, M2,..., M13) follows the seminal work of Sporns & Kötter [15]. As illustrated in the time traces for the common driving motif (M3) in the weak-coupling regime, robust synchronization between the driven nodes (1 and 3) does not occur (figure 1a), nor between directly coupled nodes (figure 1b). The lack of synchronization is also evident from the cross-correlation functions for one (figure 1c) and for an average of 40 trials (figure 1d). By contrast, strong zero-lag synchronization between these nodes (1 and 3) occurs in motifs (such as M6 and M9) that possess a reciprocal connection between at least one pair of nodes (figure 1e−l). A crucial feature of the dynamics of these synchronized motifs (M6 and M9) is that whereas the pair of edge nodes 1 and 3—which are indirectly connected via node 2—synchronize in-phase, the pairs of neighbouring nodes (1−2 and 2−3) synchronize in anti-phase at the slow rhythm. Even with a coupling delay of 10 ms, owing to the internal dynamics of the neural mass models, the phase
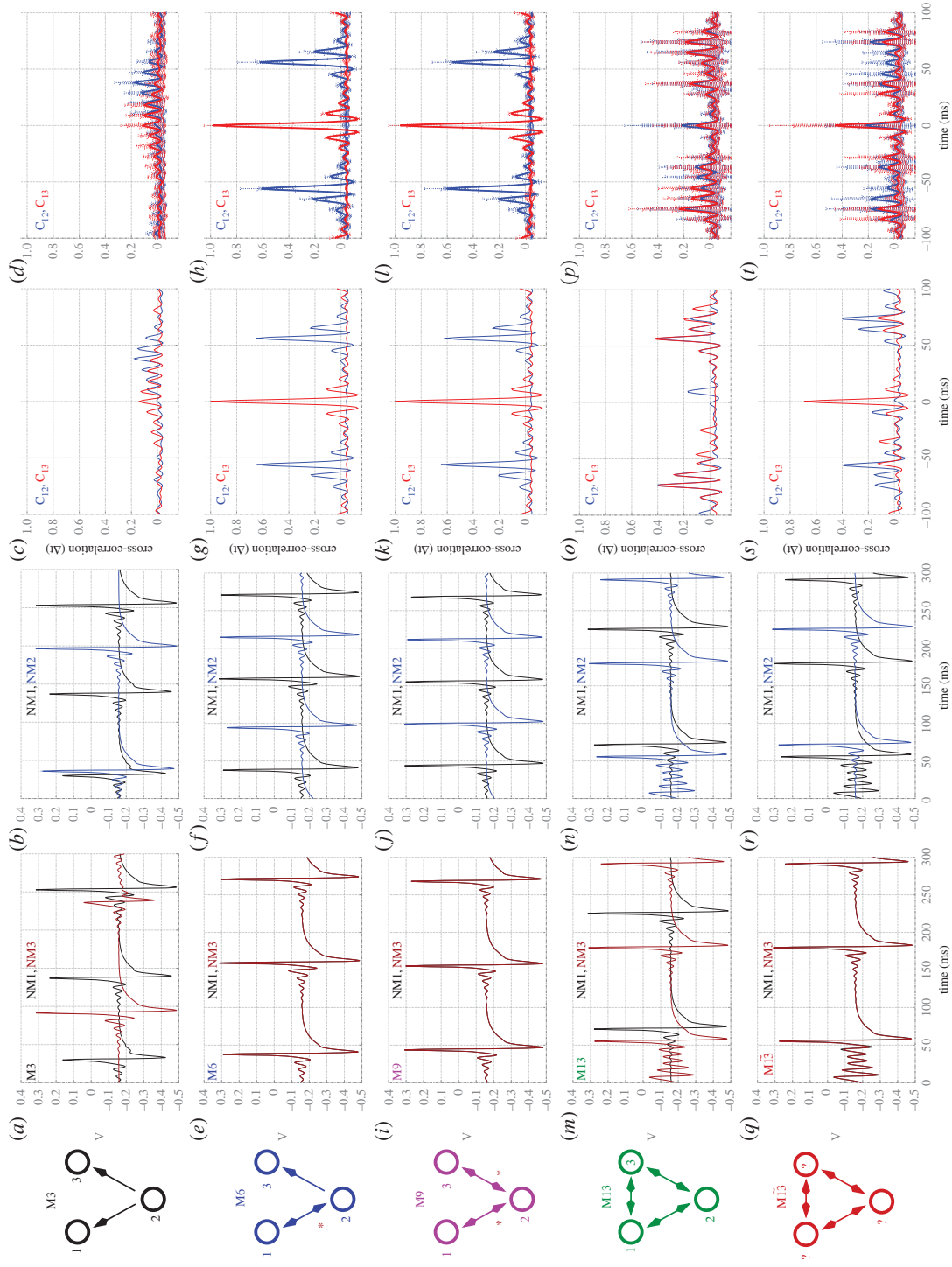
Figure 1. Synchronization in motifs of neural mass models. Dynamics of common driving motif M3 (a–d), common driving motifs with resonance pairs (tagged with red stars) M6 and M9 (e–l), and common driving motifs with frustrated resonant sources M13 and $\tilde{\text{M13}}$ (m–t) with delay $\tau = 10$ ms and coupling strength $c = 0.01$. Motif $\tilde{\text{M13}}$ has node labels determined *a posteriori* such that the zero-lag synchronization between nodes 1 and 3 is maximized. First and second columns represent time traces of individual neural mass models (1 and 3, 1 and 2, respectively), whereas the third and fourth columns represent the cross-correlation functions between node pairs of the corresponding single time series and averaged over 40 trials, respectively, with pairs 1–2 in blue and 1–3 in red. (Online version in colour.)
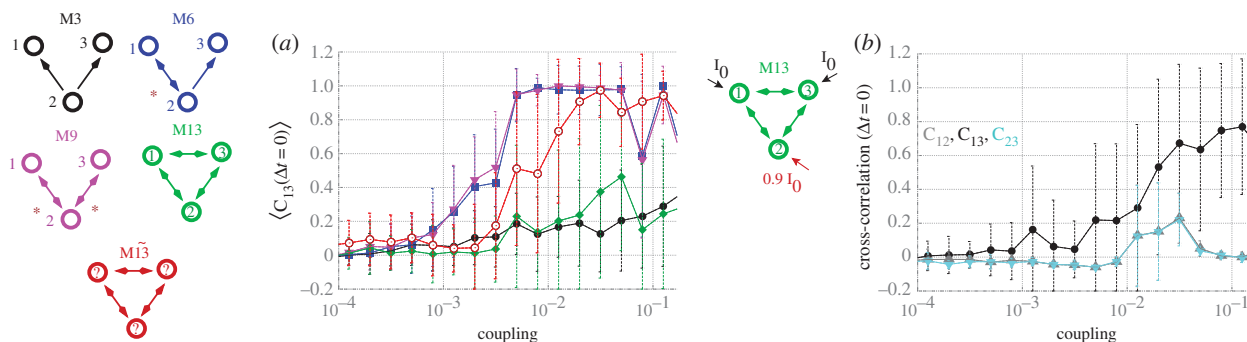
Figure 2. Frustration and symmetry breaking. (*a*) Zero-lag cross-correlation between neural masses 1 and 3 for varying coupling strength. (*b*) Zero-lag cross-correlation between pair of nodes for motif M13 with mismatch on the input current at node 2. (Online version in colour.)

difference between the neighbouring nodes amounts to about 60 ms. Hence, mutually connected nodes enhance the synchronization in these small motifs, an effect that we previously showed that can propagate along chains of connected nodes [23].

Importantly, this tendency of synchronized neighbouring nodes to oscillate in anti-phase cannot be satisfied for all motifs: for some configurations, for example when three nodes are mutually connected among themselves (motif M13), this tendency of synchronized neighbouring nodes to oscillate in anti-phase is frustrated. Typically in this motif (figure 1*m*−*p*), two out of the three pairs show anti-phase synchronization: when this happens, the third pair shows in-phase synchronization. For example, nodes 2 and 3 are in-phase for the case illustrated in figure 1*m,n*. Hence, this corresponds to an example of frustrated dynamics because although each pair shows a tendency to oscillate in anti-phase, only two out of the three pairs can accomplish this anti-phase configuration at any one time.

Starting from random initial conditions in this frustrated motif (M13), one cannot predict which pair of nodes will synchronize in phase. Hence, the average zero-lag cross-correlation across trials between nodes 1 and 3 (figure 1*i*−*l*), as well as any other pair of nodes (figure 1*p*), is markedly diminished following the incorporation of the mutual connection between nodes 1 and 3. However, the selection of whichever two nodes have the maximum cross-correlation at zero-lag after each trial (and assigning them the labels 1 and 3 *a posteriori*) reveals that the maximum zero-lag synchronization in this frustrated motif can also be strong: we called M$\tilde{1}3$ the auxiliary motif M13 that has nodes 1 and 3 labelled *a posteriori* to maximize the zero-lag synchronization between them (figure 1*q*−*t*).

4. Synchronization mode selection by symmetry breaking

The preceding analyses illustrate the effect that the resonance pair has on promoting synchronization and, conversely, how frustration destabilizes the stable state in weakly coupled small motifs. We next studied the robustness of these results with respect to the coupling strength (figure 2*a*). Nodes 1 and 3 do not show in-phase synchrony for the common driving (M3) or frustrated (M13) motifs, but they synchronize even for very weak coupling for motifs which have resonance pairs (M6 and M9). Another motif that also exhibits zero-lag synchronization between nodes 1 and 3 is motif M$\tilde{1}3$. This shows that for sufficiently strong coupling, one pair of nodes synchronizes in phase in the frustrated motif. Despite

the unpredictable character of the particular pair of nodes that synchronize when parameters across all nodes are identical, a small mismatch (such as a 10% reduction in the input current over one neural mass model) breaks the symmetry, converting the distinct node to an apex. For example, a mismatch in node 2 favours phase synchronization between nodes 1 and 3 over the other pairs 1−2 and 2−3 (figure 2*b*).

5. Synchronization on modular networks

We now focus our analyses on canonical modular structures comprising two local communities connected through a single hub. In these prototypical modular networks, we set nodes to be mutually connected with every node within each module, and the hub is mutually connected to all other nodes. Such modular structures, even for the smallest cluster size of only two nodes per module (figure 3*a*), contain frustrated motifs within clusters. In addition, this type of modular structure shares another common feature with small motifs: the hub plays the role of the apex node in motif M9, and the clusters mimic the outer nodes (figure 3*a*).

To compare synchronization in modular structures against those in motifs, we focused on the cross-correlation between two nodes belonging either to the SC or to different clusters (DCs). For each trial, the pair of nodes was selected *a posteriori* as the two nodes exhibiting maximum zero-lag cross-correlation. This was then averaged over all trials. The maximum phase synchronization between nodes belonging to DCs resembles the phase synchronization between nodes 1 and 3 in motif M9, whereas the maximum phase synchronization between nodes belonging to the SC resembles motif M$\tilde{1}3$ (figure 3*b,c*). This confirms that the motif structure is indeed influential in shaping these modular dynamics.

In the weak-coupling regime, the maximum synchronization between DCs is remarkably similar to the synchronization between nodes 1 and 3 for motif M9 (figure 3*b*). However, for stronger coupling, when the synchronization within clusters grows, the synchronization between DCs decays. As a result, the synchronization between clusters is only stronger than local synchronization for very weak coupling (see black arrow in figure 3*b*).

We next tested the role of the intra-cluster connection strength in shaping the long-distance synchronization between clusters. This was achieved by multiplying the coupling strength of the intra-cluster connection c by a weight factor $w \leq 1$. For this experiment, we used a modular structure with a larger cluster size, as shown in figure 4*a*. As illustrated in
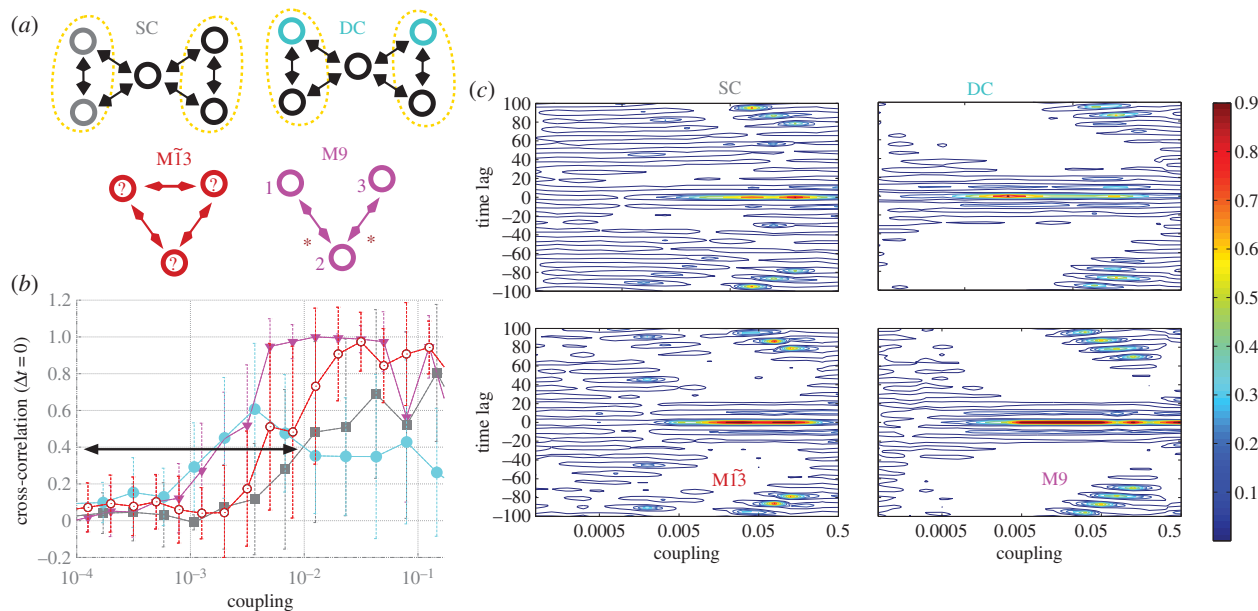
Figure 3. Zero-lag synchronization from motifs to modular structures. (a) Pairs on minimal modular structure selected from the SC and from DCs can be compared with motifs of three nodes. (b) Zero-lag synchronization of nodes 1 and 3 of motifs M9 and M$\tilde{1}$3, and maximum zero-lag synchronization between nodes located at different and SCs of modular structures. Black arrow denotes the range of weak coupling in which the synchronization is stronger between nodes of DCs than nodes of the SC. (c) Contour plot of cross-correlations for varying coupling strength and time lag. Line represents curves along which the cross-correlations have a constant value. White regions correspond to regions between contour lines, and the large white areas represent negative cross-correlation values, as can be seen in figure 1k,l for motif M9 and $c = 0.01$. Cross-correlation between nodes 1 and 3 on motif M9 (M$\tilde{1}$3) resembles the maximum cross-correlation between DC (SC) nodes. (Online version in colour.)
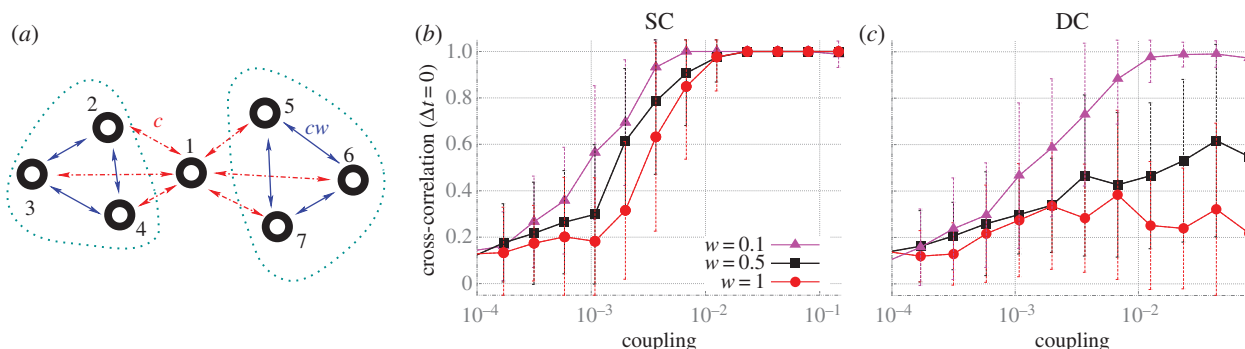

Figure 4. Maximum zero-lag synchronization in larger modular structures. (a) Canonical modular network with one hub (node 1) and two clusters (composed of nodes: 2, 3 and 4; 5, 6 and 7). The connections between hub-cluster nodes (red dotted lines) have strength c, and cluster–cluster connections (blue lines) have strength cw. (b) Maximum zero-lag synchronization between nodes from the SC. (c) Maximum zero-lag synchronization between nodes located at DCs. (Online version in colour.)

figure 4b,c, the synchronization strength increases for both SC and DC as the weight w is reduced. However, although our measures of synchronization improve for very low w, the variability of the synchrony pattern is reduced because the frustration is diminished. Hence, in the case of weak intra-cluster connectivity, the system exhibits a strong tendency to evolve to a state of global synchronization in which all cluster nodes are in phase with each other, and in anti-phase synchrony with the hub node.

Setting the weight ratio $w = 1$ and comparing the maximum zero-lag synchronization in modular structures with DC sizes (grey curve of figure 3b against red curve of figure 4b), we find that the synchronization inside a cluster is stronger for larger cluster sizes. Having the maximum synchronization inside a cluster that grows with the size is an expected result because for larger clusters, the total coupling is stronger by construction (nodes inside a cluster are all-to-

all connected), and the number of candidate pairs to synchronize also grows. On the other hand, an unexpected result appears when comparing the synchronization between clusters for DC sizes (blue curve of figure 3b against red curve ($w = 1$, dots) of figure 4c): in this case, the larger cluster gives rise to a weaker synchronization between clusters. These results indicate that for $w = 1$, there is a competition between SC and DC synchronization, in which the presence of SC synchronization prevents the synchronization between DCs.

6. Variability of synchronization patterns

Even frustrated motifs show a small set of stable patterns of synchronization. Owing to the larger number of nodes and the presence of several frustrated motifs within each cluster, modular structures exhibit a larger number of stable patterns of
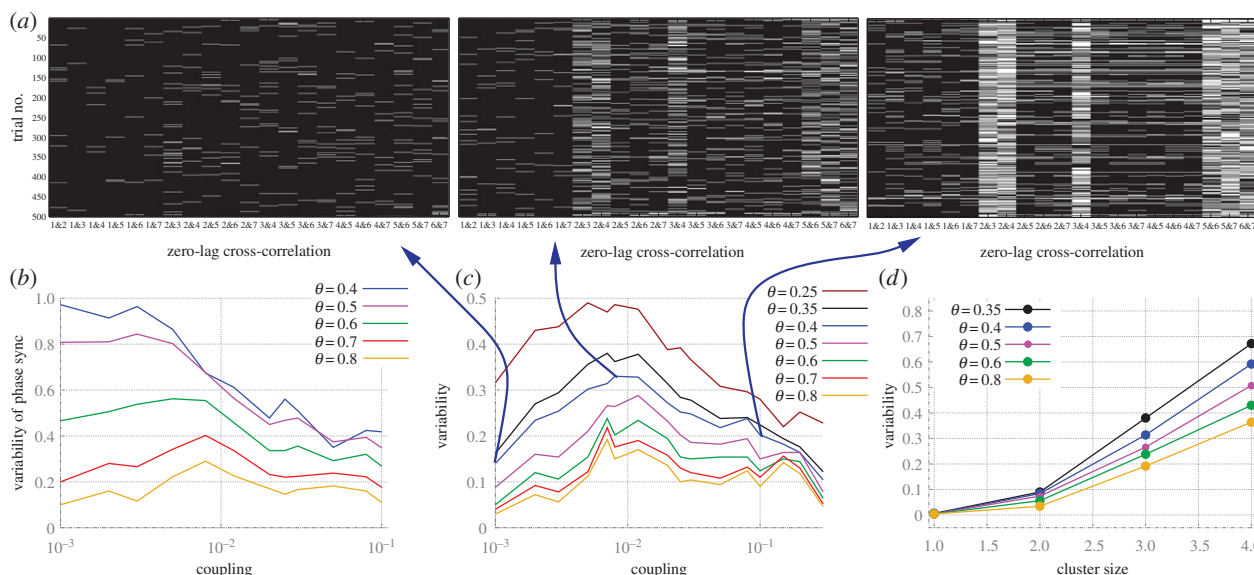
Figure 5. Quantifying the variability of synchronization patterns in modular structures. (a) Zero-lag cross-correlation above the threshold θ between pairs of nodes (labelled as per figure 4a) in 500 trials. (b) Variability of the trial-to-trial patterns of synchronization for any phase lag in modular structures with cluster size 3. (c) Same as panel (b), but restricted to zero-lag synchronization. (d) Variability of the zero-lag synchronization for modular structures with clusters of different sizes and coupling $c = 0.008$. (Online version in colour.)

synchronization. By performing multiple trials with random initial conditions, it is possible to estimate the variability of phase synchrony by counting the number of different outcomes that are found in a quasi-stationary regime.

To measure the variability of phase synchrony, we dichotomized pairs as either synchronized or not synchronized for each trial of 2 s (discarding a transient period of 500 ms) depending on whether the cross-correlation coefficient was greater than a threshold θ. Figure 5a illustrates different patterns of zero-lag synchronization obtained from the network studied in figure 4a for different coupling strengths, in which white (black) stripes represent synchronized (unsynchronized) pairs. We then estimated the variability by counting the number of different patterns and dividing by 500, the total number of trials.

The analysis of the phase synchronization—defined as the maximum cross-correlation at any lag (figure 5b)—reveals a strong dependence of the synchronization variability on the threshold θ. The appearance of a maximum synchronization variability at intermediary coupling strength is evident for sufficiently high threshold. Next, we restricted the synchronization to zero-lag phase synchronization, such that a synchronized pair is identified only if the zero-lag cross-correlation coefficient was above θ (figure 5c). Hence, we see that the zero-lag synchronization variability is also optimized for an intermediary coupling strength: the synchronization is too sparse for very weak coupling and conversely too stable for strong coupling. Moreover, as the number of nodes, resonance pairs and frustrated motifs grow with size, the maximal variability also grows with the cluster size (figure 5d).

7. Macaque cortical networks

(a) Statistical features of macaque structural networks

We first re-visit some basic network features, such as modularity and motif distribution, as expressed in cortical networks of the macaque. These will guide our structure–function

analyses. In particular, we study three binary CoCoMac networks: the visual cortex (with $N = 30$ nodes; figure 6a), the visual and sensorimotor areas (with $N = 47$ nodes; figure 6b) and the larger macaque cortical network (composed of $N = 71$ nodes; figure 6c). These are collated cortical networks of the macaque (CoCoMac [44,45]), available at the brain connectivity toolbox [18].

A modular decomposition of these networks [18,46,47] suggests that these three networks have two, four and four modules, respectively. Analyses of the frequency of structural counts of the 13 configurations of three-node motifs (figure 6d) for the macaque networks reveal substantial differences with respect to the presence of intermodular connectivity (figure 6e–g). Motifs M12 and M13 are typically composed entirely by intra-modular connections (blue bars, bottom). By contrast, motifs M4, M6 and M9 appear more often connecting inter-modular nodes, either by exclusively inter-modular connections (red bars, top) or by a combination of inter- and intra-modular connections (white bars, middle). The participation index (see appendix A), which quantifies the inter- to intra-modular connectivity ratio of each node [17,18,48], shows that many nodes with low degree exhibit strictly intra-modular connections (null participation index; lower left-hand corner of figure 6h). Conversely, high-degree nodes typically interconnect modules (upper right-hand corner). Between these extremes, there exists a tremendous variety, such that nodes of intermediate degree may connect within and/or between modules. Interestingly, network motifs also show some degree-dependent statistical patterns in these macaque networks. High-degree nodes, for example, tend to occupy the apex position of motif M9 (figure 6i) [17]. This feature suggests that nodes in the apex position of this bi-directionally connected three-node chain may play an influential role on the dynamics of distant segregated areas. Additionally, excluding nodes with very low degree, the prototypical frustrated motif M13 appears to be expressed roughly independently of the node degree (figure 6j). This indicates that although this frustrated
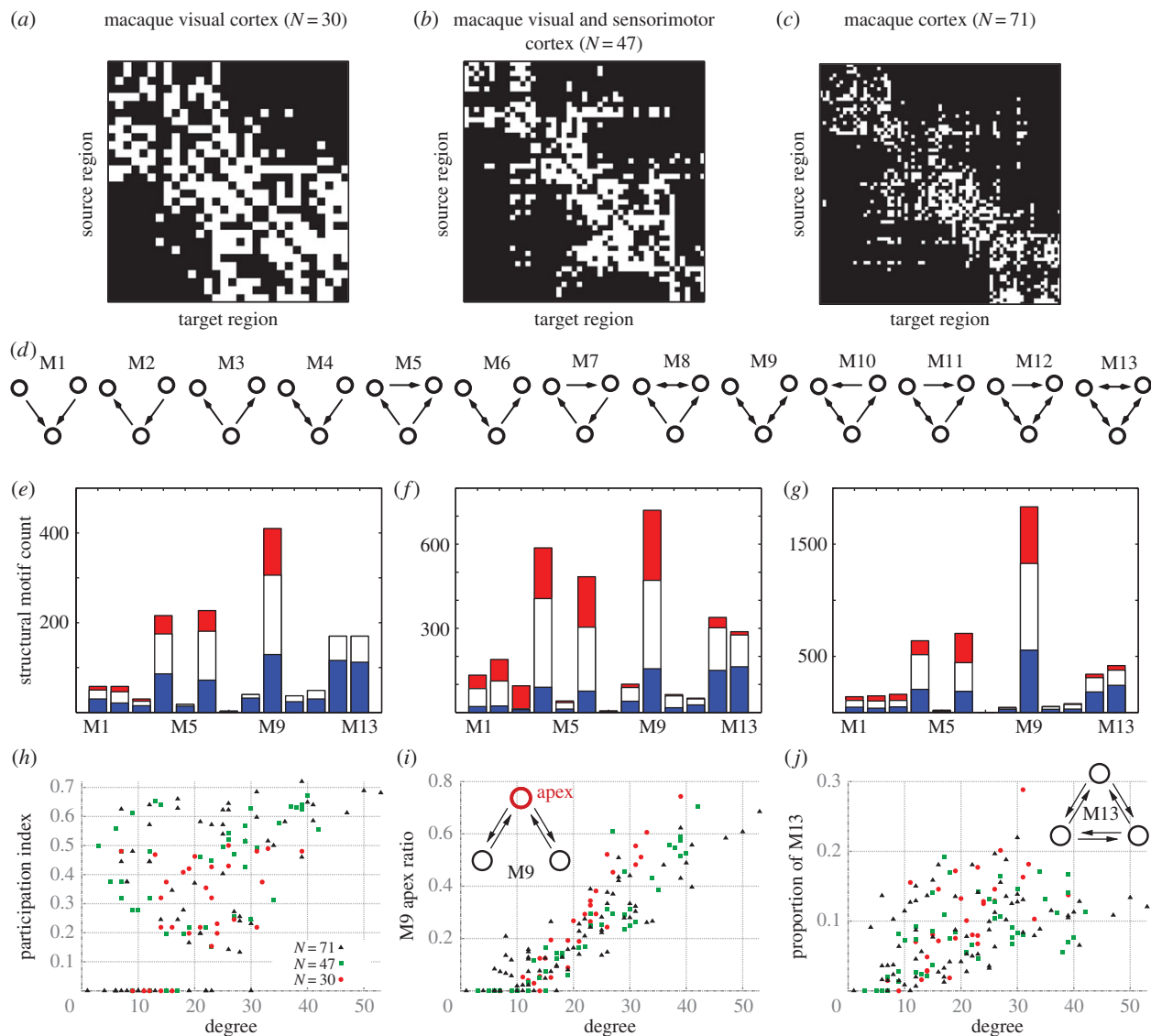
Figure 6. Motif distribution and modularity in macaque cortical networks. ($a-c$) Connectivity matrix for the different CoCoMac networks. White (black) squares indicate the presence (absence) of connections in these binary networks. (d) Three-node motifs named as per Sporns & Kötter [15]. ($e-g$) Structural motif counts (SMC) for each cortical network. The lengths of the bars denote all SMC; blue partitions (bottom) denote SMC with only intra-cluster connections; red partitions (top) denote SMC with only inter-cluster connections; white (middle) partitions denote SMC with both intra- and inter-cluster connections. (h) Scatter plot of participation index (see appendix A) and degree for each region of the three macaque networks. The degree is the sum of the number of inward and outward links. (i) Scatter plot of apex ratio for motif M9 and degree of each region. The apex ratio indicates the incidence of each region occupying the apex position of all motifs M9 in which the region takes part. Hubs (nodes with high degree) exhibit high apex ration for motif M9. (j) Scatter plot of the proportion of counts of motif M13 in which the regions participate and degree of each region. (Online version in colour.)

motif appears more often inside clusters, frustration can be a general feature affecting both hubs as well as peripheral nodes.

(b) Synchronization patterns on macaque cortex

We finally extend our analyses of the variability of synchronization patterns to these macaque cortical networks. Consistent with the dynamics on our prototypical modular networks (figure 5b), the variability of network patterns of zero-lag synchronization for the visual cortical network also exhibits a maximum for a moderate coupling strength (figure 7a). While our results have so far been restricted to a delay coupling of 10 ms, it is important to note that the coupling delay also has a strong effect in the synchronization of the network and its variability (figure 7b): maximum variability appears for short (10 ms or less) and very long (more than 40 ms) delays, with a minimum for intermediate values (15–20 ms). Also consistent

with our prototypical networks, the dynamics on the larger cortical networks exhibit a richer variability of patterns of zero-lag synchronization (figure 7c).

8. Discussion

Adaptive brain function rests upon the ability of cortical networks to balance the competing constraints of variability and stability. Using the dynamics on network motifs, we investigated the influence of structural connectivity on the diversity of synchronization patterns. We identified resonance and frustration as two major principles in sculpting the variability of the functional networks: reciprocal pairs enhance zero-lag synchronization via resonance-induced synchronization; Frustration decomposes stable synchronized dynamics into multiple competing stable solutions. Together, the two
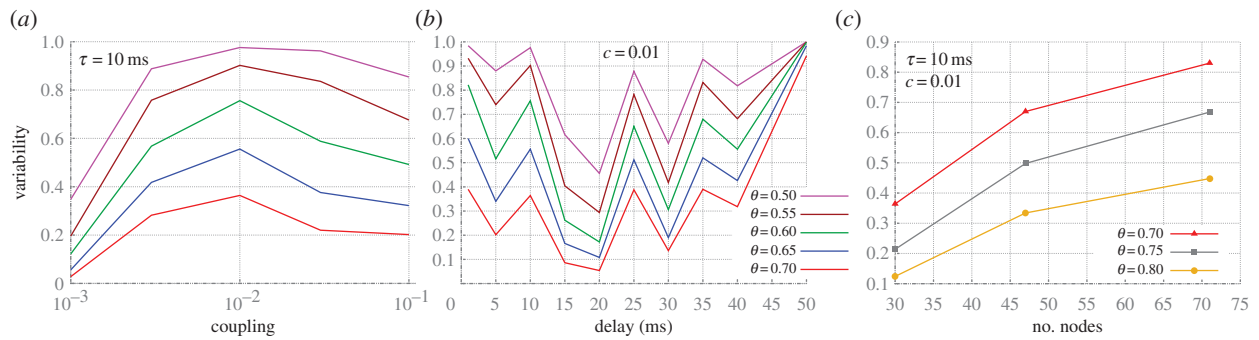
Figure 7. Variability of synchronization patterns in cortical networks. Maximum variability of zero-lag synchronization, as measured in figure 5c, for the macaque visual cortex ($N = 30$) for varying coupling strength (a), and for varying coupling delay (b). (c) Variability of zero-lag synchronization for different macaque cortical networks. (Online version in colour.)

principles appear to give rise to metastable dynamics in systems of different sizes, from motifs to cortical networks.

We propose that in larger networks, these dyadic influences reflect the contrasting deployment of these motifs with respects to their modular organization. Assuming that modules contain larger clustering, motif M13 represents a key connectivity pattern within modules. An important contribution of this frustrated motif is to enrich the dynamical landscape of synchronized cortical states. This property of frustrated systems to enrich and diversify the dynamics is general and occurs in other systems [49–53]. However, to the best of our knowledge, this is the first time it has been related to large-scale cortical dynamics.

The over-representation of motifs M9 and M6 is a consistent and characteristic property of cortical networks [15,17,23]. Taking into account that apex regions typically connect distant regions, in agreement with previous work [54–56], our results suggest that one functional role for these hubs is to promote the synchronization between segregated regions belonging to DCs. According to this proposition, these connections would enrich the variability of synchronization between clusters, which in our model occurs more sparsely than inside clusters.

Changes in brain connectivity have been associated with pathological brain states, such as schizophrenia [57] and multiple sclerosis [58]. Our results show that two crucial features of the structural connectivity that shape the cortical dynamics are the number of resonant pairs and frustrated motifs. Future work could investigate whether these two structural elements (resonant pairs and frustrated motifs) are altered in neurological and psychiatric illnesses characterized by network dysplasia [59].

In addition to changes in structural connectivity, many pathological brain states are also associated with alterations in neuronal synchrony, which may be either reduced (e.g. autism [60] and schizophrenia [61,62]) or increased in levels of synchrony (e.g. epileptic seizures [63] and Parkinson's disease [64]). A balanced amount of synchronization is an essential feature of healthy neuronal dynamics [9–11]. Consistent with experiments and simulations in networks of spiking neurons [13], our numerical analyses of large-scale oscillatory cortical (modular and macaque) networks show that the maximum variability of synchronization patterns occurs for moderate coupling: weaker coupling reduces the variability because fewer pairs can synchronize and the set of possible outcomes is restricted; stronger coupling reduces the variability because the networks often become globally

synchronized, and a smaller set of stable states is favoured over others. Such changes might plausibly underlie the reduction in consciousness associated with anaesthesia [65]. This finding of maximal variability for moderate coupling reinforces the importance of homeostatic regulatory mechanisms to maintain the brain close to its optimal region of the parameter space [11]. Our results are also consistent with prior analyses of the role of delays [12,66] and network size in shaping the cortical dynamics.

While resonance-induced synchronization has been shown to hold for synchronized pairs, regardless of their phase relation [23], frustration requires the synchronization between pairs of nodes to be in anti-phase. Anti-phase synchronization is a common phase relationship between separated cortical regions found in a variety of experimental sets [13,67] and models [23,54,68]. The phase relation of the synchronization depends on many factors such as the balance between excitation and inhibition within a cortical region [13], and the coupling strength between regions [68]. More importantly, however, anti-phase becomes the dominant regime when inter-region synapses involve a substantial conduction delay [68]. For this reason, we argue that our model, which favours anti-phase synchronization, is a suitable model for the purpose of understanding the dynamics in large-scale cortical networks, in which long-distance connections are invariably associated with conduction latencies [40]. Extension of our conclusions to other systems should fundamentally depend on whether anti-phase synchronization, the condition for frustration to occur, is the stable solution for two coupled nodes.

We have used a simple way of estimating the complexity of the landscape of cortical activity states. The advantage of this measure is that it is clear and intuitive to count the number of different possible dynamic outcomes. Future work could focus on more sophisticated measures of dynamic variability, based on the system entropy [69], phase reconfiguration [70] and the temporal dwelling in the various stable solutions [71]. Links to empirical measures of dynamic functional connectivity should also be forged [8]. In addition, while we here forge a link between motifs and modules when bridging scales, future work could focus more closely on these related larger scales (of modules) as well as the shaping influence of the largest structural backbone in the primate cortex, namely the rich club [72].

Appendix A

(a) Neural mass models

The conductance-based neural mass model we used represents a mesoscale cortical region [38], which is derived from the biophysical Morris–Lecar model [73]. After adaptation to connect areas [74] with synaptic interactions [75], it reached its most recent formulation, which is suitable for modelling whole brain activity in large-scale networks [23,36,39]. Each cortical region was described by the neural mass model of spontaneous cortical dynamics

$$
\begin{aligned}
\frac{dV^i(t)}{dt} = & -\{g_{Ca} + r_{NMDA}a_{ee}[(1-c)Q_V^i(t) \\
& + c\langle Q_V^j(t-\tau)\rangle]\}m_{Ca}(V^i(t)-V_{Ca}) \\
& - \{g_{Na}m_{Na} + a_{ee}[(1-c)Q_V^i(t) \\
& + c\langle Q_V^j(t-\tau)\rangle]\}(V^i(t)-V_{Na}) \\
& - g_K W^i(t)(V^i(t)-V_K) - g_L(V^i(t)-V_L) \\
& - a_{ie}Z^i(t)Q_Z^i + a_{ne}I_0,
\end{aligned}
\tag{A 1}
$$

$$
\frac{dZ^i(t)}{dt} = b(a_{ni}I_0 + a_{ei}V(t)Q_V^i(t))
\tag{A 2}
$$

$$
\text{and} \quad \frac{dW^i(t)}{dt} = \frac{\phi[m_K - W^i(t)]}{\tau_W}.
\tag{A 3}
$$

where V is the mean membrane potential of the excitatory pyramidal neurons, Z is the mean membrane potential of the inhibitory interneurons and W is the average number of open potassium ion channels. The neural-activation functions exhibit a sigmoidal-saturating growth with V that governs the fraction of open channels m_{ion}

$$
m_{ion} = 0.5\left[1 + \tanh\left(\frac{V^i(t)-T_{ion}}{\delta_{ion}}\right)\right].
\tag{A 4}
$$

Finally, Q_V^i and Q_Z^i are the average neuronal firing rate of excitatory and inhibitory subpopulations of region i. Assuming Gaussian distributions, they are described by the following sigmoidal activation functions:

$$
Q_V^i(t) = 0.5Q_{Vmax}\left[1 + \tanh\left(\frac{V^i(t)-V_T}{\delta_V}\right)\right]
\tag{A 5}
$$

$$
\text{and} \quad Q_Z^i(t) = 0.5Q_{Zmax}\left[1 + \tanh\left(\frac{Z^i(t)-Z_T}{\delta_Z}\right)\right].
\tag{A 6}
$$

In the above equations, the following set of parameters was used [75]: $g_{Ca}(=1.1)$, $r_{NMDA}(=0.25)$, $a_{ee}(=0.4)$, $V_{Ca}(=1)$, $g_{Na}(=6.7)$, $V_{Na}(=0.53)$, $g_K(=2)$, $V_K(=-0.7)$, $g_L(=0.5)$, $V_L(=-0.5)$, $a_{ie}(=2)$, $a_{ne}(=1)$, $I_0(=0.3)$, $b(=0.1)$, $a_{ni}(=0.4)$, $a_{ei}(=2)$, $T_{Ca}(=-0.01)$, $T_{Na}(=0.3)$, $T_K(=0)$, $\delta_{Ca}(=0.15)$, $\delta_{Na}(=0.15)$, $\delta_K(=0.3)$, $\phi(=0.7)$, $\tau_W(=1)$, $Q_{Vmax}(=1)$, $V_T(=0)$, $\delta_V(=0.65)$, $Q_{Zmax}(=1)$, $Z_T(=0)$ and $\delta_Z(=0.65)$. The above equations also include other varying parameters: the coupling strength between cortical regions c, the synaptic delay between cortical regions τ and $j(=1,\dots,N)$, which are the afferent regions of region i. Consistent with the average values reported in macaques [40], we typically used a constant delay of 10 ms. Although axonal delays between two given regions are typically distributed and specific roles have been attributed to non-homogeneous delays (e.g. to shape the EEG power spectrum [76]), as a first approximation here we consider only homogeneous delays. Small delay mismatches have been shown not to affect the synchronization in neuronal motifs qualitatively [23], but the functions of delay diversity and distributed delays remain to be investigated in large-scale network models. The model was simulated in MATLAB (Math Works) using the function dde23.

(b) Participation index

The participation index P quantifies how connected nodes are with regions belonging to other modules [17,18,48]. It is defined as

$$
P_i = 1 - \sum_{m=1}^{N_M}\left(\frac{\kappa_{im}}{k_i}\right)^2,
\tag{A 7}
$$

where the summation m runs over all identified modules N_M; k_i and κ_{im} stand for the degree of node i and the number of edges from node i to nodes within module m, respectively.

References

1. Passingham RE, Stephan KE, Kötter R. 2002 The anatomical basis of functional localization in the cortex. Nat. Rev. Neurosci. 3, 606–616.

2. Sporns O. 2010 Networks of the brain, vol. 1, p. 375. Cambridge, MA: MIT Press.

3. Honey CJ, Thivierge JP, Sporns O. 2010 Can structure predict function in the human brain? Neuroimage 52, 766–776. (doi:10.1016/j.neuroimage.2010.01.071)

4. Masquelier T, Hugues E, Deco G, Thorpe SJ. 2009 Oscillations, phase-of-firing coding, and spike timing-dependent plasticity: an efficient learning scheme. J. Neurosci. 29, 13 484–13 493. (doi:10.1523/JNEUROSCI.2207-09.2009)

5. Fries P. 2005 A mechanism for cognitive dynamics: neuronal communication through neuronal coherence. Trends Cogn. Sci. 9, 474–480. (doi:10.1016/j.tics.2005.08.011)

6. Breakspear M. 2004 'Dynamic' connectivity in neural systems: theoretical and empirical considerations. Neuroinformatics 2, 205–226. (doi:10.1385/NI:2:2:205)

7. Hutchison RM et al. 2013 Dynamic functional connectivity: promises, issues, and interpretations. NeuroImage 80, 360–378. (doi:10.1016/j.neuroimage.2013.05.079)

8. Zalesky A, Fornito A, Cocchi L, Gollo LL, Breakspear M. 2014 Time-resolved resting-state brain networks. Proc. Natl Acad. Sci. USA 111, 10 341–10 346. (doi:10.1073/pnas.1400181111)

9. Friston KJ. 2000 The labile brain. I. Neuronal transients and nonlinear coupling. Phil. Trans. R. Soc. Lond. B 355, 215–236. (doi:10.1098/rstb.2000.0560)

10. Breakspear M. 2002 Nonlinear phase desynchronization in human electroencephalographic data. Human Brain Mapp. 15, 175–198. (doi:10.1002/hbm.10011)

11. Friston K, Breakspear M, Deco G. 2012 Perception and self-organized instability. Front. Comput. Neurosci. 6, 44. (doi:10.3389/fncom.2012.00044)

12. Kutchko KM, Fröhlich F. 2013 Emergence of metastable state dynamics in interconnected cortical networks with propagation delays. PLoS Comput. Biol. 9, e1003304. (doi:10.1371/journal.pcbi.1003304)

13. Yang H, Shew WL, Roy R, Plenz D. 2012 Maximal variability of phase synchrony in cortical networks

with neuronal avalanches. *J. Neurosci.* **32**, 1061–1072. (doi:10.1523/JNEUROSCI.2771-11.2012)

14. Milo R *et al.* 2002 Simple building blocks of complex networks. *Science* **298**, 824–827. (doi:10.1126/science.298.5594.824)

15. Sporns O, Kötter R. 2004 Motifs in brain networks. *PLoS Biol.* **2**, e369. (doi:10.1371/journal.pbio.0020369)

16. Song S, Sjöström PJ, Reigl M, Nelson S, Chklovskii DB. 2005 Highly nonrandom features of synaptic connectivity in local cortical circuits. *PLoS Biol.* **3**, e68. (doi:10.1371/journal.pbio.0030068)

17. Sporns O, Honey CJ, Kötter R. 2007 Identification and classification of hubs in brain networks. *PLoS ONE* **2**, e1049. (doi:10.1371/journal.pone.0001049)

18. Rubinov M, Sporns O. 2010 Complex network measures of brain connectivity: uses and interpretations. *Neuroimage* **52**, 1059–1069. (doi:10.1016/j.neuroimage.2009.10.003)

19. Harriger L, van den Heuvel MP, Sporns O. 2012 Rich club organization of macaque cerebral cortex and its role in network communication. *PLoS ONE* **7**, e46497. (doi:10.1371/journal.pone.0046497)

20. Eguíluz VM, Pérez T, Borge-Holthoefer J, Arenas A. 2011 Structural and functional networks in complex systems with delay. *Phys. Rev. E* **83**, 056113. (doi:10.1103/PhysRevE.83.056113)

21. Zhao L, Bryce Beverlin I, Netoff T, Nykamp DQ. 2011 Synchronization from second order network connectivity statistics. *Front. Comput. Neurosci.* **5**, 1–16. (doi:10.3389/fncom.2011.00028)

22. Trousdale J, Hu Y, Shea-Brown E, Josić K. 2012 Impact of network structure and cellular response on spike time correlations. *PLoS Comput. Biol.* **8**, e1002408. (doi:10.1371/journal.pcbi.1002408)

23. Gollo LL, Mirasso C, Sporns O, Breakspear M. 2013 Mechanisms of zero-lag synchronization in cortical motifs. See http://arxiv.org/abs/13045008.

24. Bullmore E, Sporns O. 2009 Complex brain networks: graph theoretical analysis of structural and functional systems. *Nat. Rev. Neurosci.* **10**, 186–198. (doi:10.1038/nrn2575)

25. Felleman DJ, Van Essen DC. 1991 Distributed hierarchical processing in the primate cerebral cortex. *Cereb. Cortex* **1**, 1–47. (doi:10.1093/cercor/1.1.1)

26. Breakspear M, Stam CJ. 2005 Dynamics of a neural system with a multiscale architecture. *Phil. Trans. R. Soc. B* **360**, 1051–1074. (doi:10.1098/rstb.2005.1643)

27. Stam C, Van Straaten E. 2012 The organization of physiological brain networks. *Clin. Neurophysiol.* **123**, 1067–1087. (doi:10.1016/j.clinph.2012.01.011)

28. Hilgetag CC, Kaiser M. 2004 Clustered organization of cortical connectivity. *Neuroinformatics* **2**, 353–360. (doi:10.1385/NI:2:3:353)

29. Zemanová L, Zhou C, Kurths J. 2006 Structural and functional clusters of complex brain networks. *Phys. D* **224**, 202–212. (doi:10.1016/j.physd.2006.09.008)

30. Hagmann P, Cammoun L, Gigandet X, Meuli R, Honey CJ, Wedeen VJ, Sporns O, Friston KJ. 2008 Mapping the structural core of human cerebral cortex. *PLoS Biol.* **6**, e159. (doi:10.1371/journal.pbio.0060159)

31. Zamora-López G, Zhou C, Kurths J. 2010 Cortical hubs form a module for multisensory integration on top of the hierarchy of cortical networks. *Front. Neuroinform.* **4**, 1. (doi:10.3389/neuro.11.001.2010)

32. van den Heuvel MP, Sporns O. 2013 Network hubs in the human brain. *Trends Cogn. Sci.* **17**, 683–696. (doi:10.1016/j.tics.2013.09.012)

33. Bullmore E, Sporns O. 2012 The economy of brain network organization. *Nat. Rev. Neurosci.* **13**, 336–349. (doi:10.1038/nrn3214)

34. Chen Y, Wang S, Hilgetag CC, Zhou C. 2013 Trade-off between multiple constraints enables simultaneous formation of modules and hubs in neural systems. *PLoS Comput. Biol.* **9**, e1002937. (doi:10.1371/journal.pcbi.1002937)

35. Zhou C, Zemanová L, Zamora G, Hilgetag CC, Kurths J. 2006 Hierarchical organization unveiled by functional connectivity in complex brain networks. *Phys. Rev. Lett.* **97**, 238103. (doi:10.1103/PhysRevLett.97.238103)

36. Honey C, Kötter R, Breakspear M, Sporns O. 2007 Network structure of cerebral cortex shapes functional connectivity on multiple time scales. *Proc. Natl Acad. Sci. USA* **104**, 10 240–10 245. (doi:10.1073/pnas.0701519104)

37. Zhou C, Zemanová L, Zamora-López G, Hilgetag CC, Kurths J. 2007 Structure–function relationship in complex brain networks expressed by hierarchical synchronization. *New J. Phys.* **9**, 178. (doi:10.1088/1367-2630/9/6/178)

38. Breakspear M, Terry JR. 2002 Nonlinear interdependence in neural systems: motivation, theory, and relevance. *Int. J. Neurosci.* **112**, 1263–1284. (doi:10.1080/00207450290026193)

39. Honey CJ, Sporns O, Cammoun L, Gigandet X, Thiran JP, Meuli R, Hagmann P. 2009 Predicting human resting-state functional connectivity from structural connectivity. *Proc. Natl Acad. Sci. USA* **106**, 2035–2040. (doi:10.1073/pnas.0811168106)

40. Tomasi S, Caminiti R, Innocenti GM. 2012 Areal differences in diameter and length of corticofugal projections. *Cereb. Cortex* **22**, 1463–1472. (doi:10.1093/cercor/bhs011)

41. Arieli A, Sterkin A, Grinvald A, Aersten A. 1996 Dynamics of ongoing activity: explanation of the large variability in evoked cortical responses. *Science* **273**, 1868–1871. (doi:10.1126/science.273.5283.1868)

42. Poulet JF, Petersen CC. 2008 Internal brain state regulates membrane potential synchrony in barrel cortex of behaving mice. *Nature* **454**, 881–885. (doi:10.1038/nature07150)

43. Cafaro J, Rieke F. 2010 Noise correlations improve response fidelity and stimulus encoding. *Nature* **468**, 964–967. (doi:10.1038/nature09570)

44. Stephan KE, Kamper L, Bozkurt A, Burns GA, Young MP, Kotter R. 2001 Advanced database methodology for the collation of connectivity data on the macaque brain (COCoMac). *Phil. Trans. R. Soc. Lond. B* **356**, 1159–1186. (doi:10.1098/rstb.2001.0908)

45. Kötter R. 2004 Online retrieval, processing, and visualization of primate connectivity data from the CoCoMac database. *Neuroinformatics* **2**, 127–144. (doi:10.1385/NI:2:2:127)

46. Reichardt J, Bornholdt S. 2006 Statistical mechanics of community detection. *Phys. Rev. E* **74**, 016110. (doi:10.1103/PhysRevE.74.016110)

47. Leicht EA, Newman ME. 2008 Community structure in directed networks. *Phys. Rev. Lett.* **100**, 118703. (doi:10.1103/PhysRevLett.100.118703)

48. Guimera R, Amaral LAN. 2005 Functional cartography of complex metabolic networks. *Nature* **433**, 895–900. (doi:10.1038/nature03288)

49. Levnajić Z. 2011 Emergent multistability and frustration in phase-repulsive networks of oscillators. *Phys. Rev. E* **84**, 016231. (doi:10.1103/PhysRevE.84.016231)

50. Jensen MH, Krishna S, Pigolotti S. 2009 Repressor lattice: feedback, commensurability, and dynamical frustration. *Phys. Rev. Lett.* **103**, 118101. (doi:10.1103/PhysRevLett.103.118101)

51. Kaluza P, Meyer-Ortmanns H. 2010 On the role of frustration in excitable systems. *Chaos* **20**, 043111. (doi:10.1063/1.3491342)

52. Nisoli C, Moessner R, Schiffer P. 2013 Colloquium: artificial spin ice: designing and imaging magnetic frustration. *Rev. Mod. Phys.* **85**, 1473. (doi:10.1103/RevModPhys.85.1473)

53. Nixon M, Ronen E, Friesem AA, Davidson N. 2013 Observing geometric frustration with thousands of coupled lasers. *Phys. Rev. Lett.* **110**, 184102. (doi:10.1103/PhysRevLett.110.184102)

54. Vicente R, Gollo LL, Mirasso CR, Fischer I, Pipa G. 2008 Dynamical relaying can yield zero time lag neuronal synchrony despite long conduction delays. *Proc. Natl Acad. Sci. USA* **105**, 17 157–17 162. (doi:10.1073/pnas.0809353105)

55. Gollo LL, Mirasso C, Villa AEP. 2010 Dynamic control for synchronization of separated cortical areas through thalamic relay. *NeuroImage* **52**, 947–955. (doi:10.1016/j.neuroimage.2009.11.058)

56. Gollo LL, Mirasso CR, Atienza M, Crespo-Garcia M, Cantero JL. 2011 Theta band zero-lag long-range cortical synchronization via hippocampal dynamical relaying. *PLoS ONE* **6**, e17756. (doi:10.1371/journal.pone.0017756)

57. Zalesky A, Fornito A, Seal ML, Cocchi L, Westin CF, Bullmore ET, Egan GF, Pantelis C. 2011 Disrupted axonal fiber connectivity in schizophrenia. *Biol. Psychiatry* **69**, 80–89. (doi:10.1016/j.biopsych.2010.08.022)

58. Coombs BD, Best A, Brown MS, Miller DE, Corboy J, Baier M, Simon JH. 2004 Multiple sclerosis pathology in the normal and abnormal appearing white matter of the corpus callosum by diffusion tensor imaging. *Mult. Scler.* **10**, 392–397. (doi:10.1191/1352458504ms1053oa)

59. Bullmore E, Frangou S, Murray R. 1997 The dysplastic net hypothesis: an integration of developmental and dysconnectivity theories of

schizophrenia. *Schizophr. Res.* **28**, 143–156. (doi:10.1016/S0920-9964(97)00114-X)

60. Wilson TW, Rojas DC, Reite ML, Teale PD, Rogers SJ. 2007 Children and adolescents with autism exhibit reduced meg steady-state gamma responses. *Biol. Psychiatry* **62**, 192–197. (doi:10.1016/j.biopsych. 2006.07.002)

61. Breakspear M, Terry J, Friston K, Harris A, Williams L, Brown K, Brennan J, Gordon E. 2003 A disturbance of nonlinear interdependence in scalp EEG of subjects with first episode schizophrenia. *Neuroimage* **20**, 466–478. (doi:10.1016/S1053-8119(03)00332-X)

62. Spencer KM *et al*. 2003 Abnormal neural synchrony in schizophrenia. *J. Neurosci.* **23**, 7407–7411.

63. Steriade M. 2003 *Neuronal substrates of sleep and epilepsy*. Cambridge, UK: Cambridge University Press.

64. Uhlhaas PJ, Singer W. 2006 Neural synchrony in brain disorders: relevance for cognitive dysfunctions and pathophysiology. *Neuron* **52**, 155–168. (doi:10. 1016/j.neuron.2006.09.020)

65. Murphy M *et al*. 2011 Propofol anesthesia and sleep: a high-density EEG study. *Sleep* **34**, 283.

66. Deco G, Jirsa V, McIntosh A, Sporns O, Kötter R. 2009 Key role of coupling, delay, and noise in resting brain fluctuations. *Proc. Natl Acad. Sci. USA* **106**, 10 302–10 307. (doi:10.1073/pnas. 0901831106)

67. Canolty RT, Ganguly K, Kennerley SW, Cadieu CF, Koepsell K, Wallis JD, Carmena JM. 2010 Oscillatory phase coupling coordinates anatomically dispersed functional cell assemblies. *Proc. Natl Acad. Sci. USA* **107**, 17 356–17 361. (doi:10.1073/pnas. 1008306107)

68. Li D, Zhou C. 2011 Organization of anti-phase synchronization pattern in neural networks: what are the key factors? *Front. Syst. Neurosci.* **5,** 100. (doi:10.3389/fnsys.2011.00100**)**

69. Deco G, Jirsa VK. 2012 Ongoing cortical activity at rest: criticality, multistability, and ghost attractors. *J. Neurosci.* **32**, 3366–3375. (doi:10.1523/JNEURO SCI.2523-11.2012)

70. Breakspear M, Williams LM, Stam CJ. 2004 A novel method for the topographic analysis of neural activity reveals formation and dissolution of dynamic cell assemblies. *J. Comput. Neurosci.* **16**, 49–68. (doi:10.1023/B:JCNS.0000004841.66897.7d)

71. Freyer F, Roberts JA, Ritter P, Breakspear M. 2012 A canonical model of multistability and scale-invariance in biological systems. *PLoS Comput. Biol.* **8**, e1002634. (doi:10.1371/journal.pcbi.1002634)

72. van den Heuvel MP, Sporns O. 2011 Rich-club organization of the human connectome. *J. Neurosci.* **31**, 15 775–15 786. (doi:10.1523/JNEUROSCI.3539-11.2011)

73. Morris C, Lecar H. 1981 Voltage oscillations in the barnacle giant muscle fiber. *Biophys. J.* **35**, 193–213. (doi:10.1016/S0006-3495(81)84782-0)

74. Larter R, Speelman B, Worth RM. 1999 A coupled ordinary differential equation lattice model for the simulation of epileptic seizures. *Chaos* **9**, 795–804. (doi:10.1063/1.166453)

75. Breakspear M, Terry JR, Friston KJ. 2003 Modulation of excitatory synaptic coupling facilitates synchronization and complex dynamics in a biophysical model of neuronal dynamics. *Network Comput. Neural Syst.* **14**, 703–732. (doi:10.1088/0954-898X/14/4/305)

76. Roberts JA, Robinson PA. 2008 Modeling distributed axonal delays in mean-field brain dynamics. *Phys. Rev. E* **78**, 051901. (doi:10.1103/PhysRevE.78.051901)